JOURNAL OF MATERIALS SCIENCE 37 (2002) 3765–3776

Interfacial reactions of zirconium and zirconium-alloy liquid metals with beryllia at elevated temperatures

S. M. McDEAVITT
Chemical Technology Division, Argonne National Laboratory, Argonne, Illinois, USA
E-mail: mcdeavitt@cmt.anl.gov

G. W. BILLINGS
West CERAC, Inc, McCarran, NV 89434, USA

J. E. INDACOCHEA
CME Department, University of Illinois at Chicago, Chicago, Illinois, USA

Argonne National Laboratory and Integrated Thermal Sciences, Inc. are developing crucible materials for melting reactive metals. A major part of this effort involves identifying reusable materials because they would have little or no interaction with the molten metals at elevated temperatures. Sessile drop-type experiments have been performed using pure zirconium and stainless steel-zirconium alloys (e.g., HT9-15Zr) on beryllia (BeO) substrates. The system was heated in high-purity argon to about 2000°C, held for 5 minutes, and cooled to room temperature. An external video camera monitored the interfacial interaction and wetting behavior. The zirconium melted and wetted the BeO at 1600°C, far below its melting point (1855°C). Post-test examinations show beryllium and oxygen dissolving in the zirconium metal. In addition, zirconium infiltrated the BeO substrate. No third phase reaction product was present at the zirconium-beryllia interface either at the top of the substrate or in the infiltrated region. HT9-15Zr also reacted with BeO; the alloy infiltrated partially into the BeO and formed a reaction-like layer attached to the ceramic substrate at the interface with the solidified metal. The rest of the liquid metal alloy did not wet the reaction product band. The results indicate that BeO is a poor crucible for the present application, but the observed wetting and infiltration phenomena are relevant to understanding the behavior of the liquid metal-ceramic interfaces.

1. Introduction

The control of interface reactions between dissimilar materials is a significant issue in such applications as designing ceramic-metal composites, brazing ceramics, and melting reactive metals in refractory crucibles. In ceramic/metal systems interfacial reactions are often accompanied by wetting of the ceramic surface by the liquid metal. Wetting is defined, in general, as a condition in which the interfacial tension between a liquid and a solid is such that the contact angle, θ, is less than 90°. In systems where wetting is not expected from simple surface tension considerations, θ is greater than 90°. Thus, at elevated temperatures, the contact angle of a liquid metal on a ceramic is expected to be a good indicator of whether an interfacial reaction has occurred [1].

Chemical reactions between ceramics and liquid at elevated temperatures can lead to the formation of undesirable phases at the solid-liquid interface. The question of interface design and control for these materials is complex and many parameters affect the structure of the interface either as it evolves during processing or as it results from the liquid metal/ceramic contact, depending on the application. For example, in joining silicon nitride and silicon carbide ceramics with nickel-based superalloys, a favorable interface must be created to guarantee a sound joint. Extensive chemical reactions occur if these materials are in intimate contact at elevated temperatures for extended periods of time, which result in the formation of metal silicides [2–5]. Research on metal-matrix composites with silicon carbide has shown that the interfacial reaction sequence and ultimate morphology are mainly dependent on the materials selected [6–8], and these features have a direct relationship to the composite's performance.

Therefore, material selection is critical to the engineering of the interface structure to produce the desired bulk properties. The characterization of an individual ceramic/metal interface provides helpful data that can be used as criteria in controlling the interface properties and phase evolution [9]. A recent study states the need to characterize the factors governing the reaction pathways at these interfaces [10]. This information can

be used to design diffusion paths that will inhibit formation of undesirable phases or maintain the stability of the ceramic surface in our crucible application.

The atomic or electronic structure of the metal is a significant factor that affects the reactivity of the liquid metal in contact with the ceramic material. However, the thermal energy and materials' properties (e.g., solubility and surface energy) are also important aspects that influence this liquid metal/ceramic material interaction. Sessile-drop studies of wetting on silicon carbide (SiC) showed lack of wetting by metals with low or moderate melting temperatures, e.g., Pb, Sn, Ag, or Au [11, 12], indicating minimal interaction. On the other hand, ferrous metals and pure nickel have been shown to wet SiC moderately [11–13], but this wetting is accompanied by a significant dissolution of SiC in the liquid metal [13–15].

Argonne National Laboratory and Integrated Thermal Sciences, Inc., are presently developing crucible materials for melting zirconium, stainless steel-zirconium alloys, and other reactive metals. Our objectives are to identify materials that can be reused with little or no interaction with the molten metals at elevated temperatures and to understand the reactions that occur at the metal/ceramic interface. The test metals included high purity zirconium and ferritic stainless steel-zirconium alloys, (i.e., SS-15 wt% Zr and Zr-8 wt% SS). These alloys are of interest because our primary application is to produce them as high-level nuclear waste form [16]. Pure zirconium was tested to isolate its behavior, because it is the most reactive component in the SS-Zr alloys. This paper presents results pertaining to Zr and HT9-15Zr on beryllium oxide (BeO). Substrate selection was based on the relative thermodynamic stability of the oxides with respect to ZrO_2 by a simple comparison of the Gibbs free energy of formation.

A literature survey of the compatibility of metals with refractory oxides [17] in an inert atmosphere below 1400°C, revealed that beryllia among other oxides (titania, magnesia, zirconia, alumina and thoria) remained unaffected when exposed to metals such as titanium, zirconium, niobium, and others. Economos and Kingery [17] observed, however, that some interfacial reactions with various metals, including Zr, started to be appreciable at 1600°C and became significant at 1800°C.

2. Interfacial metal-ceramic reactions and wetting

The characterization of a metal/ceramic interface requires an understanding of the energetics of wetting and interface chemical reactions, as well as the microstructure and composition of interface compounds. Chemical wetting occurs when an electronic exchange occurs across the liquid/solid interface by virtue of chemical bonds [18]. That is, chemical bonds are formed as the electronic structure of the surface atoms of the two mating surfaces is modified. This modification takes place by one of two mechanisms: reduction/oxidation (redox wetting) or by dissolution and mixing of one phase into the other.

In a sessile-drop experiment, a drop of liquid metal rests on a flat ceramic surface. The shape of the drop is recorded and these measurements may be used to compute the surface tension of the liquid metal, γ_{LV}, together with the contact angle of the drop on the flat surface, θ, defined in Fig. 1. This schematic exemplifies poor wetting condition. The contact angle θ is represented by the Young equation, which is derived by a simple force balance:

$$\gamma_{SV} + \gamma_{LV} \cdot \cos(180^\circ - \theta) = \gamma_{SL} \tag{1}$$

or,

$$\cos\theta = \frac{\gamma_{SV} - \gamma_{SL}}{\gamma_{LV}} \tag{2}$$

It is known that θ is affected by the substrate geometry and roughness [19], the chemical composition of the phases present, and the vapor pressure of the phases. For example, the oxygen partial pressure has been shown to affect the measured value of θ in metals that form a strong oxide layer at their surface [20, 21]. This change occurs because of the oxide formation at the metal drop surface that prevents proper contact between metal and substrate.

When a reaction phase is produced at the interface of the liquid metal and the ceramic substrate, a new configuration develops (Fig. 2), which is described as reactive wetting. According to Laurent [21], the smallest contact angle in a reactive system is expressed by:

$$\cos\theta_{min} = \cos\theta_0 - \frac{\Delta\gamma_R}{\gamma_{LV}} - \frac{\Delta G_R}{\gamma_{LV}} \tag{3}$$

where, θ_0 is the contact angle of the liquid metal on the ceramic substrate in the absence of any reaction, $\Delta\gamma_R$ is the change in interfacial energies brought about by the interfacial reaction, (this term accounts for the change in the nature of the interface that results from the interfacial reaction), and ΔG_R is the change in free

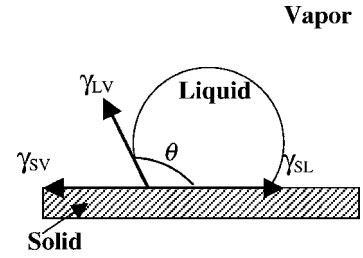

Figure 1 Schematic of solid substrate poorly wetted by a molten-metal droplet.

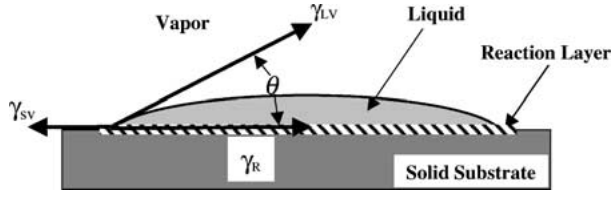

Figure 2 Schematic of a solid substrate wetted by liquid metal with formation of a reaction layer. The sketch shows good wetting characteristics.

energy per unit area released by the reaction of material contained in the vicinity of the metal/ceramic interface. The term $(\Delta G_R/\gamma_{LV})$ in Equation 3 was proposed on the reasoning that the reaction between the liquid and an unreacted ceramic surface at the periphery of the drop increases the driving force for wetting [22–25].

For interface reactions that produce no new phase at the interface and involve only dissolution of the ceramic substrate into the melt, divergent opinions exist regarding the influence of ΔG_R on wetting [24, 27]. This is due in part to the kinetic complexities involved in the theory of reactive wetting and to difficulties in evaluating ΔG_R and measuring the contact angle. Calculated values of ΔG_R are said to be very sensitive to the choice of thickness of the effective interface, that is, the number of atomic layers constituting the zone in which the diffusionless reaction occurs [28]. Experimental data exhibiting an effect of ΔG_R on wetting by a metal are somewhat sparse, as indicated by Naidich [23] and Pask [26]. Most of the analyzed experimental data from reactive sessile drop experiments have been described without considering ΔG_R, and just in terms of changes in the nature of the metal/substrate interface, along with other effects such as the shape of the reaction products, and the kinetics of reaction that accompany the reaction [29, 30].

A way to take advantage of the interfacial reactions as a means of promoting wetting without causing massive reactions between the metal and the ceramic, is to alloy a non-reactive base metal with controlled quantities of reactive solute additions. This approach is used to design filler metal brazing alloys for ceramics [24, 27, 29], and is well illustrated by the case of Al_2O_3 and SiO_2 wetted by nickel containing a reactive alloy addition [30].

3. Experimental procedure

High-temperature experiments were performed by placing small samples of solid metal on ceramic substrates in the configuration shown in Fig. 3, heating the sample to temperatures above the metal melting point and observing the behavior of the system. The goals for these sessile drop-style experiments were (1) to screen stable ceramics as candidate crucible materials for melting reactive metals and (2) to observe the wetting and high-temperature interactions between the molten metals and ceramic substrates. The work reported here is one segment of an ongoing study of metal/ceramic interfaces at high temperature.

Oxides and other ceramics were fabricated from high-purity powders (99.9%) by hot uniaxial pressing (HUP). Single-component oxides (e.g., BeO, Y_2O_3, MgO, and CaO) were fabricated, along with several stable mixed oxides (e.g., $MgAl_2O_4$, $CaZrO_3$, $CaO \cdot HfO_2$, and $MgO \cdot ZrO_2$). Substrate selection was based on the relative thermodynamic stability of the oxides with respect to ZrO_2 by a simple comparison of the Gibbs free energy of formation, ΔG_f (Fig. 4). Oxides with ΔG_f higher than that of ZrO_2 were automatically disqualified since Zr metal will reduce them. It was recognized that even oxides with ΔG_f below ZrO_2 could react with the liquid metals because of complexities that arise at high temperatures. The hot-pressed substrates all had densities above 85% theoretical density; most were in the range of 92 to 95% theoretical density. The surface state of the ceramic substrate was in the as-processed condition, and no other surface modifications were done.

Up to four metal-ceramic combinations were heated in a given experiment (Fig. 3). All materials were cleaned prior to the tests; acetone was used to remove dirt and other contaminants from the materials, and then dried completely before the heating cycle. The metal specimens used in this portion of our investigation were pure Zr (99.5%, with Hf as the major contaminant at 0.16% by weight, carbon, chromium, tin, sulfur and iron) and a ferritic stainless steel (HT9) alloyed with

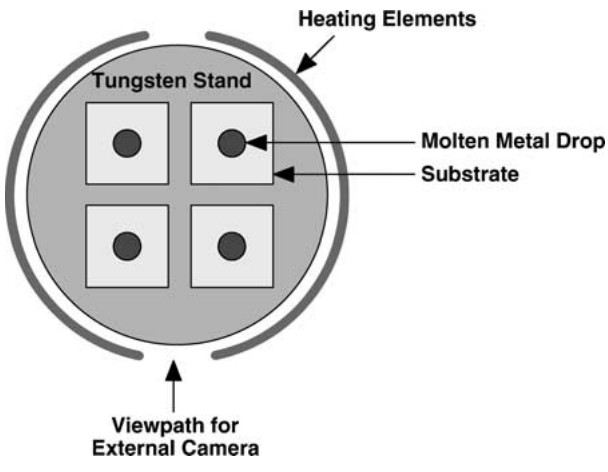

Figure 3 Experimental set-up of sessile-type test. Top view.

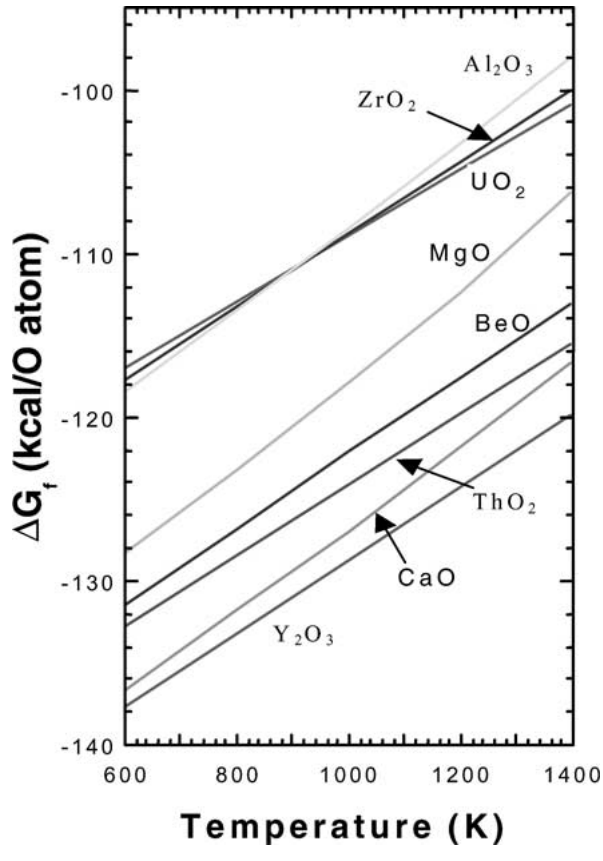

Figure 4 Gibbs free energies of formation for selected oxide ceramics.

15-wt% Zr, a material referred to as HT9-15Zr. The composition of the HT9 metal (in weight percent) is 0.5Ni, 12.0Cr, 0.2Mn, 1.0Mo, 0.25Si, 0.5W, 0.5V, 0.2C, and balance Fe.

The sample stage was heated in a tungsten mesh furnace in high-purity argon (research grade, 99.99% purity). A sensing thermocouple was placed about 0.5 cm beneath the samples. The materials were preheated at about 600°C, and then the temperatures were ramped to the maximum test temperature, which typically exceeded 2000°C. The initial furnace ramp was 20°C/min from 600°C to an intermediate temperature of 1600°C for the HT9-15Zr alloy and 1800°C for Zr. From there, the ramp was slowed to 10°C/min, and heating continued to the peak temperature. For the HT9-15Zr alloy, the temperature was increased manually after 1600°C, because its low melting point of 1350°C. In most cases, the samples were held at the peak temperature for ~5 minutes and then cooled at ~200°C/min to 1200°C, where the furnace was shut-off.

An external video camera was used to view the interaction and wetting behavior of the samples and to record the experiment, as shown in Fig. 3. The view path for the camera was through a small window in the furnace and between the split in the tungsten mesh furnace elements. A series of welding glass plates were used to filter the intense radiant light from the furnace hot zone while viewing the experiment progress. *In situ* observations were followed by post-test examinations using scanning electron microscopy (SEM) and energy dispersive spectroscopy (EDS).

4. Results and discussion

Before analysis of the data obtained in this study, we would like to point out that the melting point of the two metals used, to understand the types of reactions that occurred at different temperatures during the thermal cycle. The HT9-15Zr alloy is a eutectic material that melts between 1320°C and 1350°C. Zirconium was expected to melt near its reported melt temperature of 1855°C, unless prior reaction with the substrate affected its melting characteristics. While precise measurements of the contact angle were difficult because of the elevated temperatures and physical changes at the interface, the interfacial changes of the two systems discussed in this paper are presented in the sections that follow.

4.1. Interfacial reactions in the Zr/BeO system

Fig. 5 shows a series of video images from the Zr/BeO interaction experiment. The image at 600°C shows the parallelepiped shape of the metal sample at the start of the experiment. During heating, some surface crust developed in the Zr near the interface with BeO as the temperature approached 1500°C. At about 1550°C, a significant reaction was observed between the Zr metal and the BeO substrate. This reaction intensified and bubbling, or gas evolution, was observed at the solid-liquid boundary as the temperature reached 1580°C. At around 1605°C a liquid layer was evident at the interface, yet the Zr metal was far below its melting point

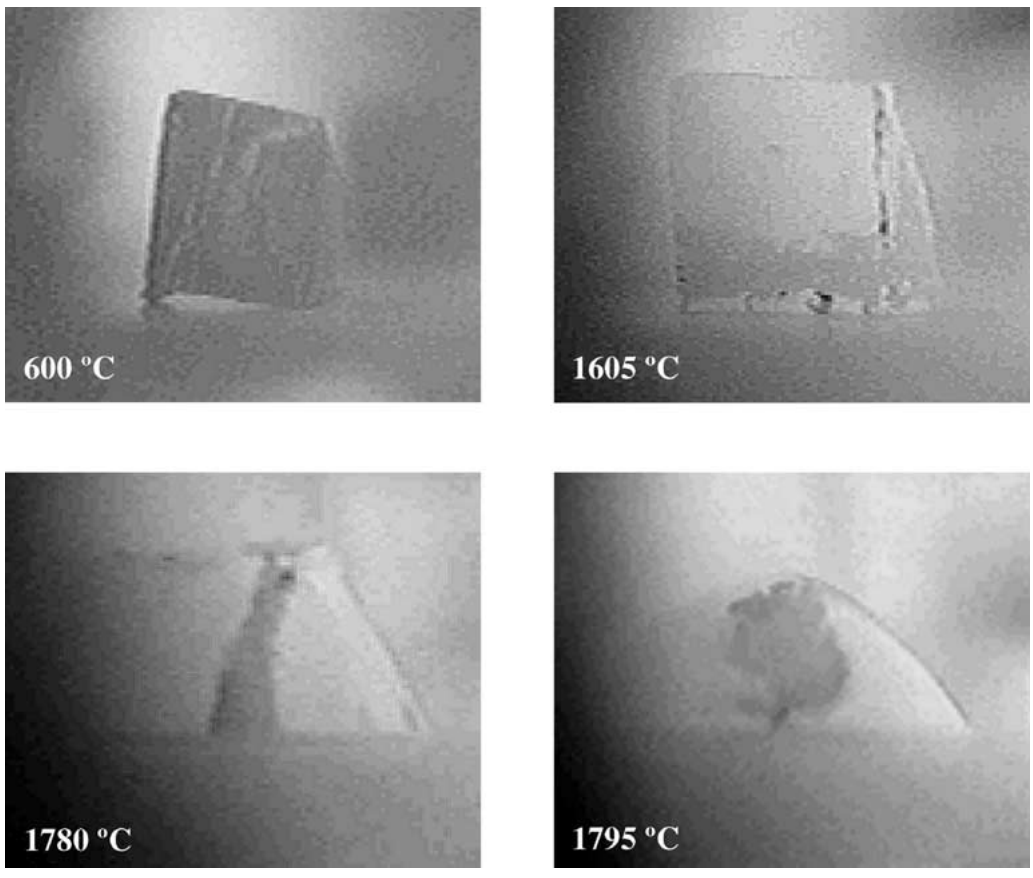

Figure 5 Video images showing the pure Zr sample as it melted on the BeO ceramic.

and the sample maintained its parallelepiped shape. As the temperature reached 1735°C, the Zr metal became distorted and assumed a trapezoid-like shape. At about 1780°C, the Zr specimen became greatly deformed because of an increased amount of liquid within the sample. At 1790°C, the Zr metal specimen collapsed and a hemispherical droplet formed. A wetting angle of approximately 60° was measured at 1795°C in a still video image (Fig. 5). The contact angle decreased significantly at ∼1825°C. The heating cycle continued up to near 2000°C, where the system was held for five minutes.

4.1.1. Chemical reaction between Zr and BeO

A chemical reaction at the Zr/BeO interface was observed by the gas evolution perceived at the liquid metal ceramic interface. The video image at 1605°C in Fig. 5 confirms this gas evolution. It is apparent that Zr has reduced BeO. One possible chemical reaction could be written as:

$$\frac{1}{2}Zr_{(s)} + BeO_{(s)} = \frac{1}{2}ZrO_2 + Be \qquad (4)$$

The Gibbs free energy of the reaction was calculated at the temperature of 1600°C, which corresponds to the temperature where melting of the Zr metal was first detected. Based on the information from thermochemical tables [31, 32], the energies of formation of 1 mole of BeO and 1/2 mole of ZrO_2 are 103.4 kcal and 91.3 kcal respectively. This results in a total Gibbs free energy change for the reaction of about +12.1 kcal. This large positive energy value makes reaction (4), as written, unlikely to occur.

Another chemical reaction that was considered to explain the chemical interaction is that of Zr reducing BeO, and then the oxygen and beryllium simultaneously dissolve in the Zr metal (α-Zr up to 863°C and then β-Zr). This reaction can be represented as follows:

$$BeO_{(s)} + Zr_{(s)} = Zr(O) + Be_{[Zr(O)]} \qquad (5)$$

The energy of formation of BeO, as indicated above, is 103.4 kcal. To obtain the corresponding energy for Zr(O) we looked at the equilibrium phase diagram of zirconium and oxygen [33], (Fig. 6), and estimated the equilibrium concentration of oxygen in α-Zr(O) to be about 16.7 at.%. With this information and referring to the thermochemical tables [31], we obtain $\Delta H_{Zr(O)} = -137$ kcal/mole, and $\Delta S_{Zr(O)} = -20$ kcal/K mole. Then $\Delta G_{Zr(O)} = -101.0$ kcal. Consequently the total Gibbs free energy change for reaction (5) is +2.4 kcal. This value, although still positive, is five times lower than the corresponding value for the chemical reaction (4). Based on these energy calculations, of the two chemical reactions written above, reaction (5) is the most likely to occur. Further evidence in support of this reasoning is found in the change of the microstructure of the Zr metal, which shows a microstructure consisting of several features typical of an alloy material, and different to the single-phase microstructure typical of a pure metal. Details of the microstructure development and/or transformations are described in Section 4.1.3. Note that the solubility of O in α-Zr is always greater than in β-Zr, but in both cases this solubility is greater than that of Be in α-Zr or β-Zr (Fig. 7 [34]). The solubility of Be is larger in β-Zr than α-Zr.

Further thermodynamic calculations of the energy of formation of Zr(O), yielded the most negative values

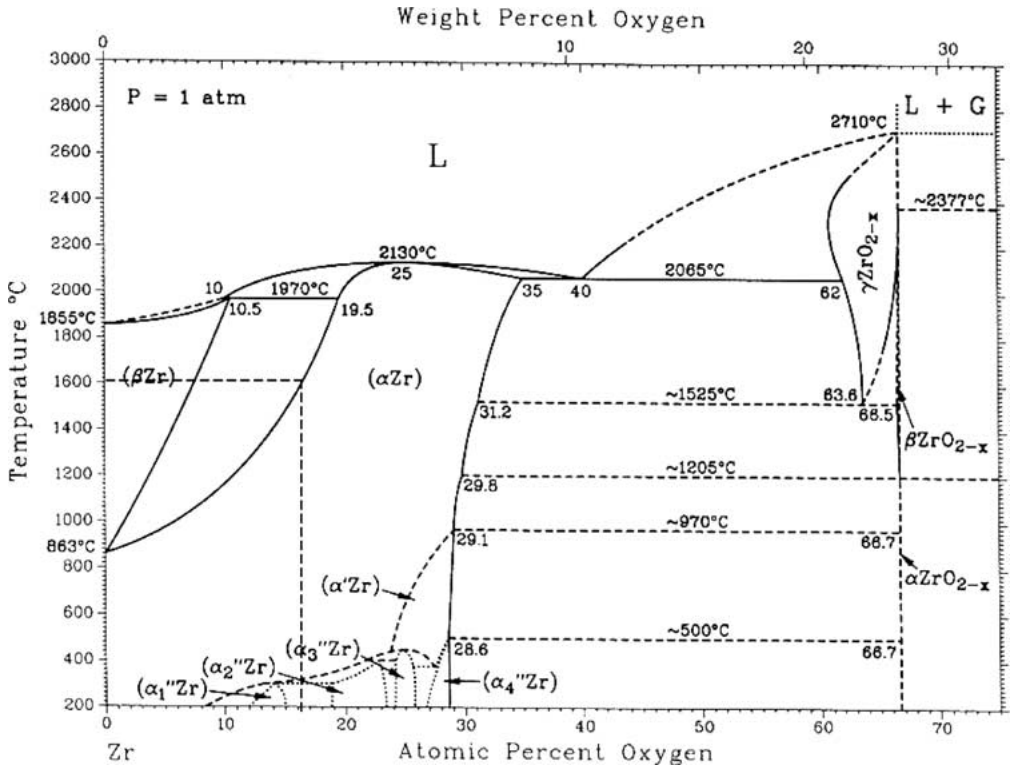

Figure 6 Equilibrium Zr-O phase diagram [33].

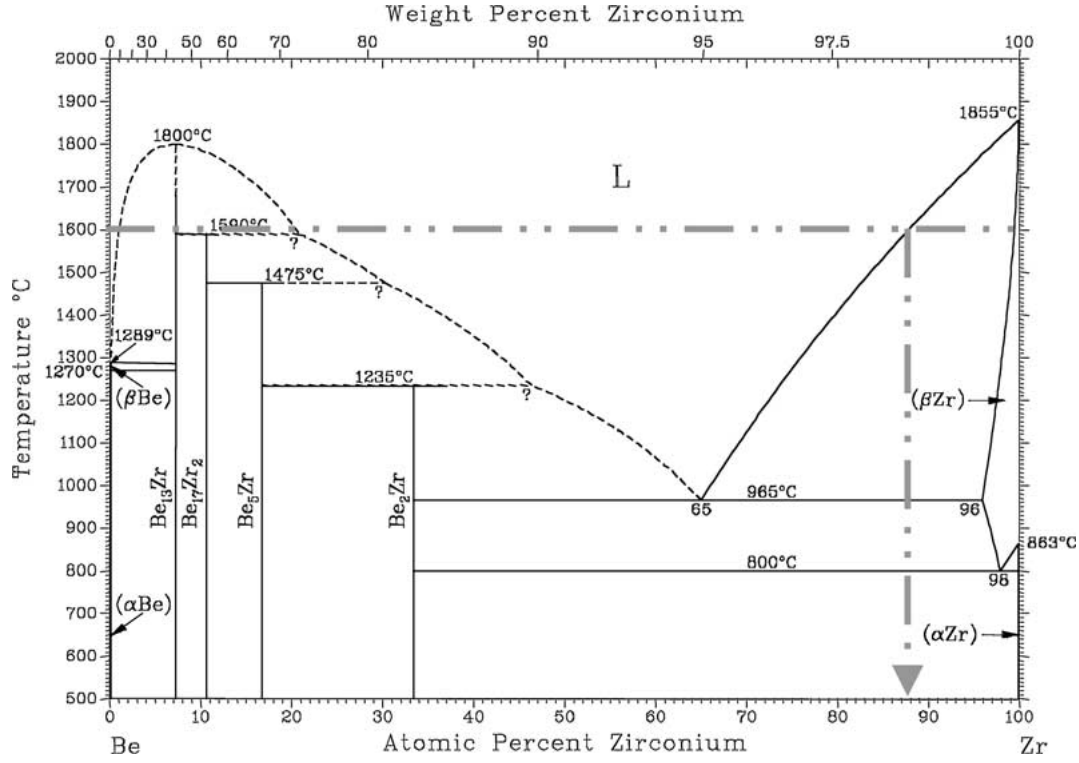

Figure 7 Equilibrium Be-Zr phase diagram [34].

ranging from −99.5 to −101.0 kcal/mole, corresponding to oxygen levels of 15.3 to 23.1 at.%. Estimates at concentrations of O above or below this range, produced less negative values. The chemical analysis by EDS of three locations of the Zr matrix offered an average value of about 10 at.% oxygen dissolved in the solidified metal. These measurements were based on a standardless analysis. If we consider 10 at.% to be the oxygen content of the Zr in the matrix, the equilibrium phases present at about 1600°C (Fig. 6) are β-Zr and α-Zr, with compositions of oxygen of 7 and 17 at.%, respectively.

4.1.2. Wetting and infiltration characteristics

Fig. 8 displays the cross section of the final shape of the Zr droplet and the BeO substrate. The ultimate wetting angle is difficult to measure because the original surface of the beryllia, represented by the dotted line in Fig. 8a, was dissolved. This observation is confirmed by the new metal/ceramic interface that receded into the beryllia. This change suggests significant dissolution of the beryllia in Zr the metal. Further, this solubility provides the mechanism for removal of the reaction products from the interface and accounts for the smoothness of the Zr/BeO interface (Fig. 8a and c). The Zr metal infiltrated the substrate, penetrating almost two-thirds of the of the 2.5 mm substrate.

The molten Zr on the top surface did not appear to spread across the BeO. The contact area at the metal/ceramic interface was approximately the same from the beginning of melting until the experiment was stopped. This behavior contrasts with the infiltration of liquid Zr into the substrate, where capillary effects would also help the spreading. It is known that oxygen in liquid metals can act as a surface-active agent that lowers the surface tension [31]. Thus, the penetration of the molten Zr-Be alloy into the beryllia may be aided by its higher concentration of oxygen at these locations, because of its proximity to the interface reaction. The infiltration of the liquid metal alloy is also influenced by the lower melting point of the Zr-Be alloy as more Be is dissolved in the alloy (Fig. 7).

4.1.3. Characterization of the microstructure

Fig. 8b shows the microstructure of the Zr metal on top of the ceramic substrate following chemical reactions and solidification. The white phase is α-Zr, the black precipitates are BeO, and the lamellae-like microstructure is a eutectic structure. EDS was used to identify the composition of the microstructure features. Fig. 9 depicts the α-Zr matrix and a BeO precipitate and identifies the locations of the spots for which a semi-quantitative (standardless) analysis was performed. Table I shows the O and Zr content of the different spots. Spots 1, 2, and 4 correspond to the α-Zr matrix, where the oxygen was measured at about 10.0 at.%. The primary constituent at these spots is Zr; Be is expected to have dissolved in this matrix, but this element is too light to be detected by the equipment used.

TABLE I EDS standardless analysis of microconstituents in Zr-metal of the Zr/BeO system (at.%)

	Spot number[a]				
Element	1	2	3	4	5
Oxygen	9.0	10.0	100.0	10.0	96.0
Zirconium	91.0	90.0	–	90.0	4.0

[a]See Fig. 9.

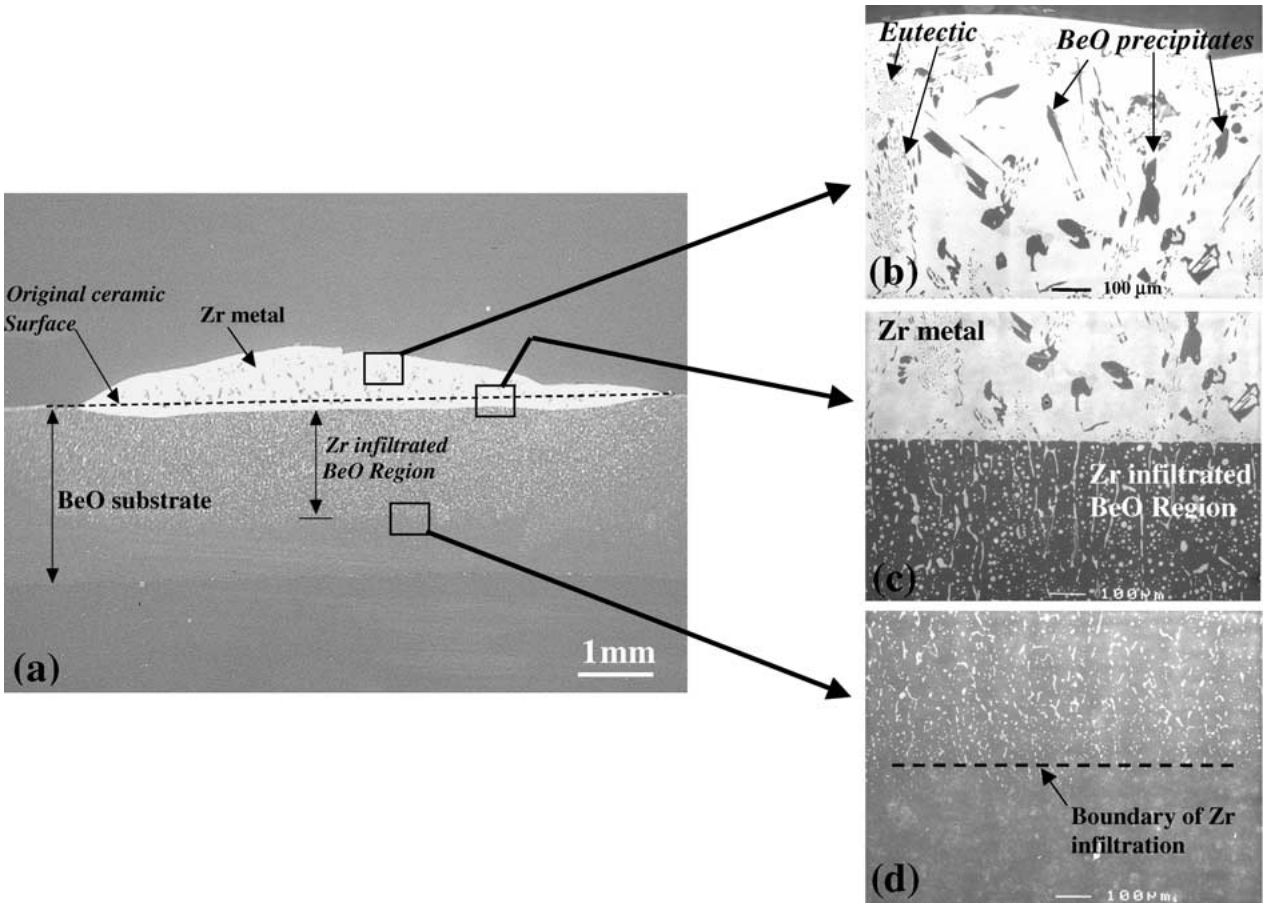

Figure 8 Interface between the Zr metal and the beryllia substrate following solidification of the system. Composite figure shows details of microstructure for three regions. No reaction phase precipitated at the metal-ceramic interface.

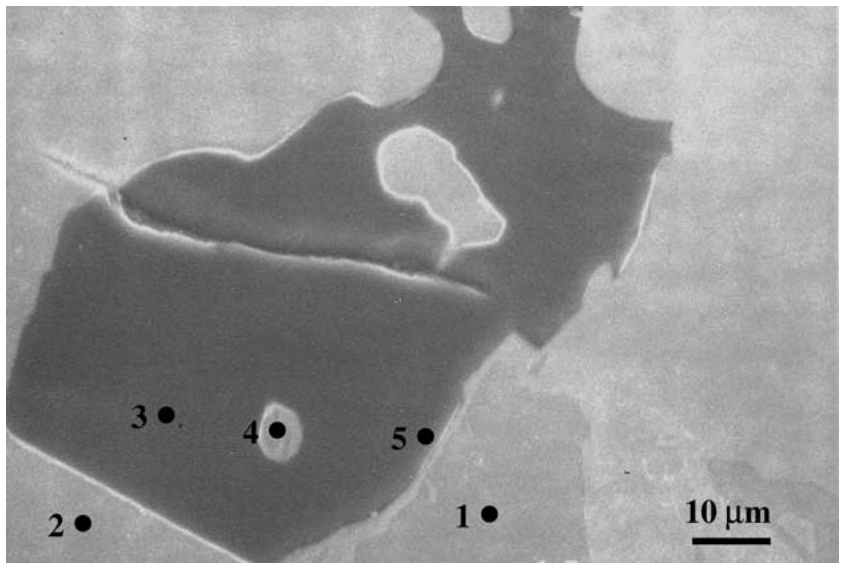

Figure 9 SEM micrograph showing the α-Zr matrix and BeO precipitate and locations of the EDS spot analyses.

The compositions of the spots in Fig. 9 reported in Table I, particularly in the Zr matrix, are consistent with what is predicted by the equilibrium phase diagrams in Figs 6 and 7. Zr has limited solubility for Be: for example, at 800°C the maximum solubility of Be in β-Zr is 2 at.% but almost negligible in α-Zr. The coarser, blocky, black phase in the microstructure (Figs 8b and 9) is BeO. The EDS analysis of this phase (point 3 in Fig. 9 and Table I) shows only oxygen and no Zr; Be must be present but it is too light to be detected by the instrument. BeO precipitates during solidification of the liquid metal by the oxidation of the excess Be before the eutectic reaction. Notice that Zr is virtually insoluble in β- and α-Be. Concurrent with the BeO precipitation, β-Zr also forms (Fig. 7).

Fig. 8b shows the fine eutectic microstructure. According to the Be-Zr phase diagram (Fig. 7), there is only one eutectic reaction, which occurs in the Zr end

of the phase diagram at about 965°C. In our system, we hypothesize that pure Zr is being alloyed by the Be reduced from the BeO. Thus, the phase transformations must follow equilibrium changes in the Zr rich portion of the phase diagram. Liquid was observed at the Zr/BeO interface at about 1600°C, hence Be must have alloyed the Zr, for it to melt below 1855°C. According to the phase diagram (Fig. 6), for Be-Zr liquid to be in equilibrium with Zr at this temperature, the liquid alloy must contain about 12 at.% Be and Zr must be present as β-Zr and contain ~0.5 at.% Be. These results indicate that the Be-Zr alloy formed is a hypoeutectic alloy, where the equilibrium composition of the eutectic alloy would be Zr-35 at.% Be.

Note that the reduction of BeO by Zr produces Be and O and both of these elements dissolve in liquid Zr. However, as the solubility limits of both elements in Zr is exceeded, the free Be will react with the excess O to produce new BeO. Thus, as the temperature reaches the eutectic temperature the phases present will be β-Zr, BeO particles, and eutectic Be-Zr liquid alloy. O would also be in solution in β-Zr and in the eutectic. When temperature drops below ~965°C, a eutectic transformation will occur (Fig. 7); the eutectic microstructure consists β-Zr and the intermetallic Be_2Zr. Both phases are expected to have O dissolved in them. EDS analysis of the black phase of the eutectic was done to confirm the intermetallic Be_2Zr. In the BeO precipitated prior to the eutectic reaction, only oxygen was detected and no Zr was measured. Spot chemical analyses on three particles of the eutectic intermetallic (acicular-like dark phase) revealed the presence of Zr (17–20 at.%) and oxygen. The detection of Zr in these eutectic microconstituents suggests that these are indeed Be-Zr intermetallics.

4.2. Interfacial reactions in the HT9-15Zr/BeO system

The HT9-15Zr/BeO system was heated to a peak temperature of 2016°C, where it was held for five minutes and then cooled at a rate of about 200–300°C/min to 1200°C, where the furnace was shut-off and the cooling was uncontrolled to room temperature. During heating partial melting was detected near the interface at ~1340°C, while the remaining solid block floated away from the interface. As the temperature reached ~1350°C, a non-wetting hemispherical cap was formed in contact with the interface. Still, a solid lump was present within the molten cap (Fig. 10 indicated by an arrow), and the sample retained this shape even as the temperature approached 2016°C. Segregation or slag entrapment was observed at the location indicated by the arrow.

4.2.1. Chemical reaction between HT9-15Zr and BeO

The interfacial reactions and melting characteristics in this system were different than those observed in Zr/BeO. In the video no interfacial reaction was evident before melting. The HT9-15Zr alloy has a melting point (the eutectic temperature is ~1335°C) lower than the temperature at which the chemical reaction was observed in the Zr/BeO system. Thus, the eutectic melting preceded the interfacial reaction between Zr and BeO, blocking it from view in the video as the temperature of the system approached 1500°C. The reaction band that formed and remained attched to the BeO, however, gives evidence of a chemical reaction, as seen in Figs 10 and 11. Region 2 in both figures is the reaction band.

The interface reaction between the HT9-15Zr alloy and the BeO occurred by Zr reducing the beryllia. An EDS spot analysis of the reaction band, and not the infiltrated metal alloy, showed Zr and O, but Be is also expected.

4.2.2. Wetting and infiltration characteristics

The metal alloy did not wet the ceramic substrate; the contact angle was larger than 90°, as seen in Fig. 10. This lack of wetting occurred despite the formation of a reaction region. The infiltration of the alloy into the reaction band did not reduce the wetting angle either.

Fig. 11 (Region 2) shows clearly the infiltration of the liquid alloy into the ceramic substrate, behavior similar to that of the Zr/BeO system. But the penetration of the HT9-15Zr into the BeO was not as extensive in this case: ~200 μm, compared to a penetration of ~1600 μm for pure Zr (Fig. 8). Note that the penetration of the liquid HT9-15Zr into the ceramic substrate only extends through the thickness of the reaction band (Fig. 11b). The lower infiltration depth of the metal alloy than the pure zirconium into the substrate may be attributed to the content of Zr. The Zr, it seems, acted as the wetting agent that allowed the HT9 alloy to spread and infiltrate into the pores and cavities of the BeO substrate. A smooth and almost straight horizontal boundary is defined between the beryllia and the reaction product, yet the original BeO interface has receded, as seen in Fig. 11a. This confirms the dissolution of the beryllia. Only the cavities or pores in the reaction band are filled with the HT9-15Zr alloy. None of the pores in the beryllia substrate adjacent to the interface were observed to be filled with the metal alloy.

4.2.3. Characterization of the microstructure

The separation of Regions 1 and 2 (illustrated in Figs 10 and 11) suggests a difference in composition, structures, and physical properties. It is apparent that the coefficients of thermal expansion of regions 1 and 2 are quite different. Fig. 12 exhibits the typical solidification microstructure of a cast HT9-15Zr alloy, consisting of dendrites and a eutectic microstructure. This structure was found in the droplet above the BeO. The same microstructure was also found in the liquid metal that infiltrated the BeO, (Region 2 in Fig. 11 and Fig. 13). This cast microstructure has been discussed in detail in a previous publication [16]. Region 2 of Fig. 11 is practically a composite material with a ceramic matrix (gray phase in Fig. 11b) and infiltrated metal. The interface between Region 2 and the bulk BeO is well defined by the depth of the liquid penetration (Fig. 11b).

A chemical characterization across the interface between the two regions was performed via EDS (Fig. 13). The results from the spot analyses are tabulated and are

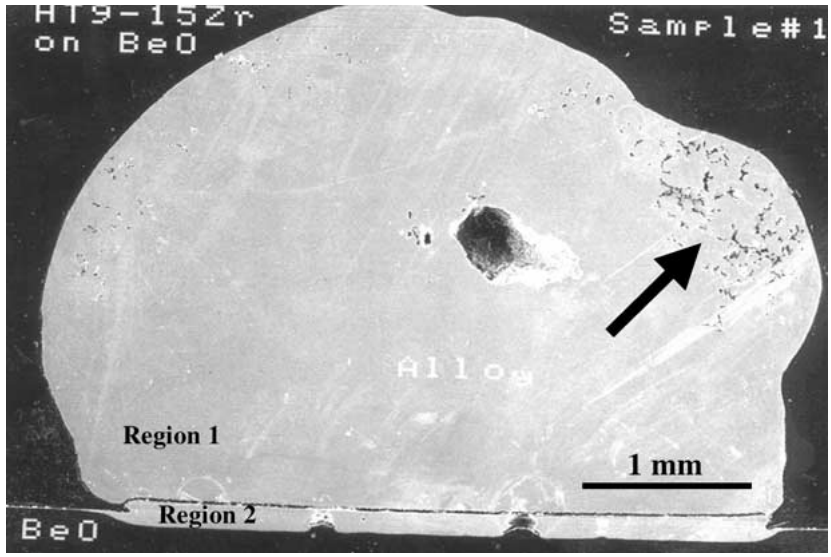

Figure 10 SEM micrograph showing the vertical cross section of HT9-15Zr alloy droplet on BeO. Arrow points to region of segregation.

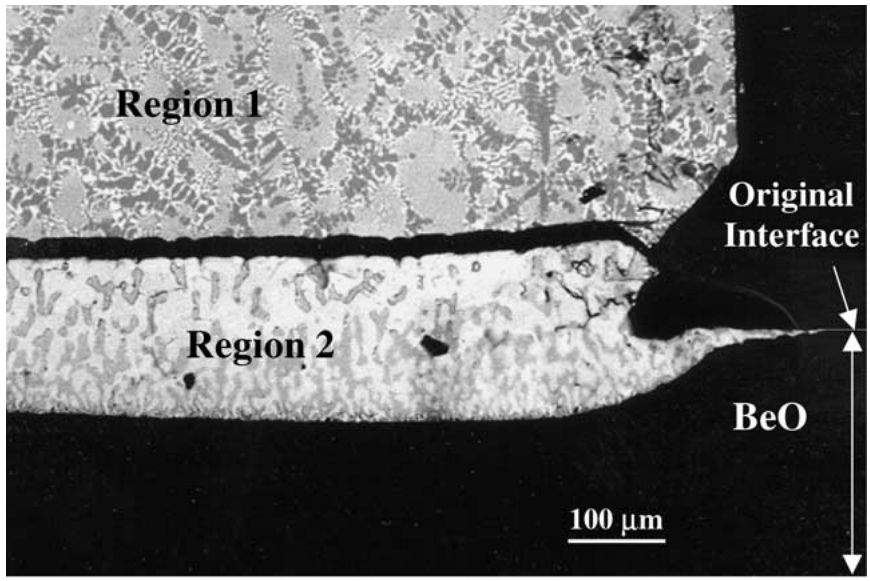

(a)

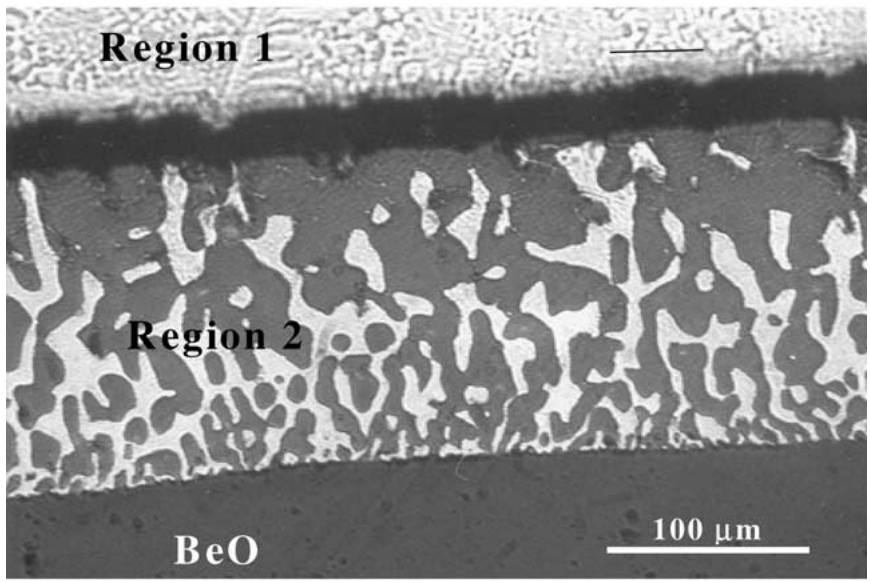

(b)

Figure 11 Alloy HT9-15Zr and BeO interface following melting at 2016°C and cooling to room temperature: (a) SEM micrograph and (b) optical micrograph.

TABLE II ESD spot analysis at interface of HT9-15Zr/BeO system and bulk chemistry of HT9 steel

	Spot number[a]										
	1		2		3		4		5		HT9
Element	at.%	wt%	at.%	wt%	at.%	wt%	at.%	wt%	at.%	wt%	wt%
O	9.3	2.9	0.0	0.0	45.3	12.8	7.7	2.4	11.8	3.3	–
Zr	0.1	0.1	35.2	47.1	53.8	86.4	0.8	1.3	16.6	26.7	–
Fe	76.7	82.9	58.9	48.3	0.6	0.6	77.9	82.8	61.9	61.0	85.4
Cr	13.5	13.6	5.1	3.9	0.1	0.1	13.3	13.2	9.1	8.3	11.5
Ni	0.4	0.5	0.8	0.7	0.1	0.1	0.3	0.3	0.6	0.6	0.6
Mn	0.0	0.0	0.0	0.0	0.0	0.0	0.0	0.0	0.0	0.0	0.7

[a]See Fig. 13.

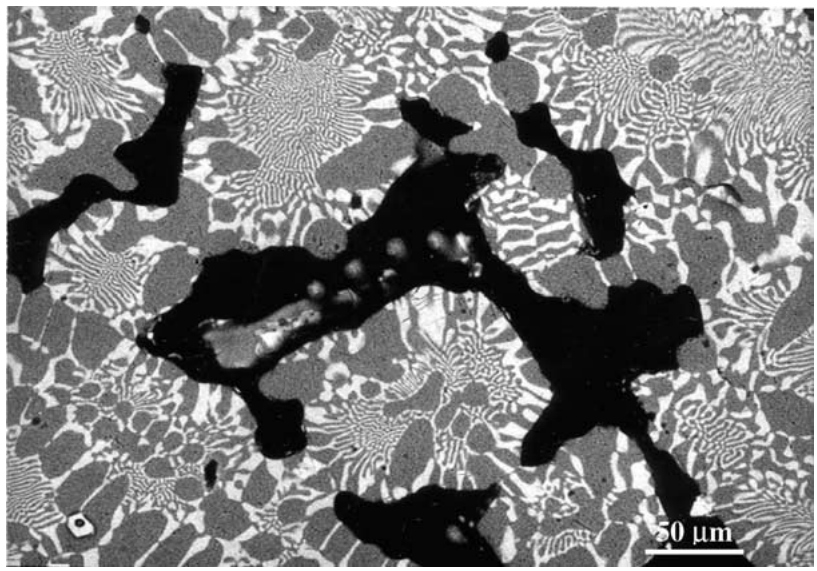

Figure 12 Solidification microstructure of the HT9-15Zr alloy showing location of segregation.

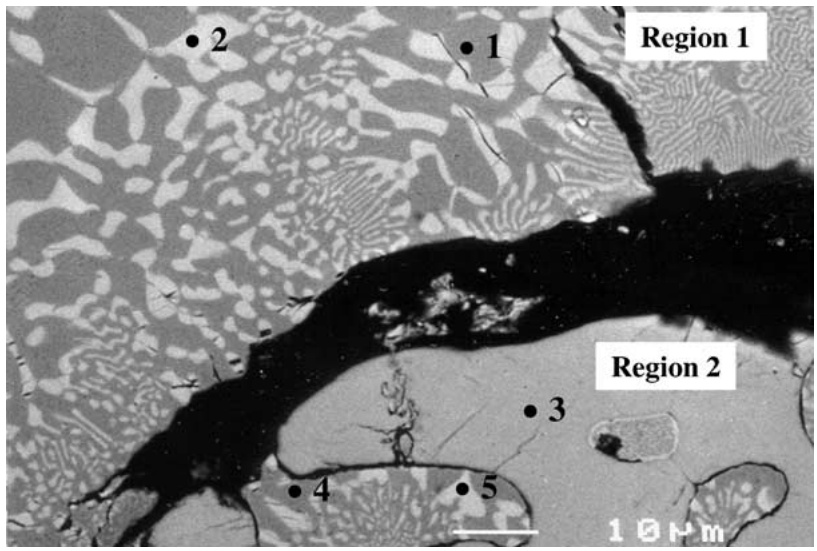

Figure 13 SEM micrograph of the HT9-15Zr/BeO interface. The black dots represent the EDS spot analyses at both sides of the interface.

presented in Table II. Again, beryllium is not reported because it is too light to be identified by EDS. Spot #3 corresponds to the matrix of the ceramic reaction band (Region 2 in Fig. 13); it contains Zr (∼54.0 at.%) and O (∼45.0 at.%); however, Be must be present also. The excessive content of Zr at this region confirms the reduction of the BeO by Zr. Clearly, Zr diffused preferentially to this region to react with BeO to form a compound of Zr, Be, and oxygen. Unlike pure Zr, no BeO precipitates were found either in the solidified droplet or infiltrated metal, possibly because Be is more soluble in iron or chromium than in pure zirconium.

Spots 1 and 4 reveal an iron-rich (α-Fe, ferrite) matrix with chromium and oxygen in solid solution. However, Be is likely present too because Fe and Cr are the main elements of the matrix and both have notable solubility for Be. Spots 2, and 5 correspond to the white intermetallic phase of the metal alloy, $Zr_x(Fe, Cr, Ni)_y$. Both of these spot analyses display comparable chemistries; however there is some difference in the

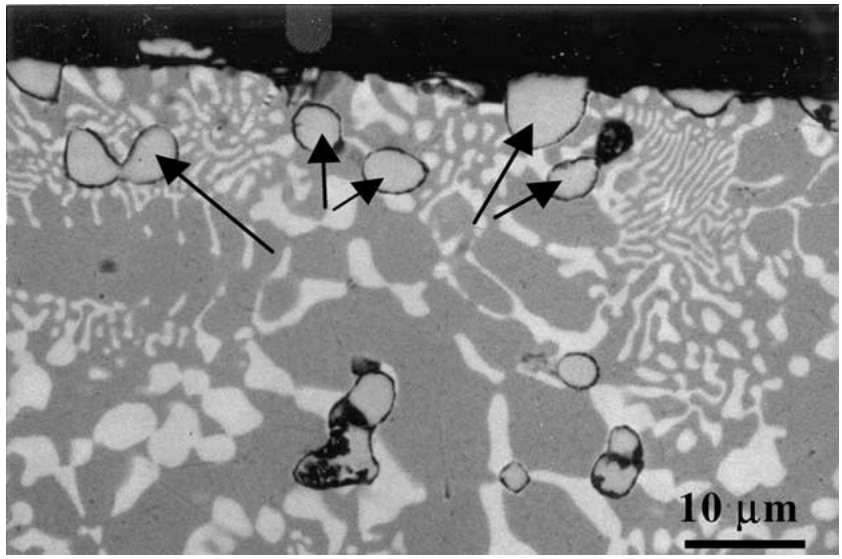

Figure 14 Segregation of non-soluble particles to the top of the solidified alloy droplet.

levels of oxygen and zirconium between both spots. Spot 5 contained oxygen (11.8 at.%), while no oxygen was found in spot 2. The value corresponding to oxygen in spot 5 could also include Be. In addition, Be forms an intermetallic with Zr (Fig. 7), as explained earlier. Consequently the white intermetallic phase, particularly in the infiltrated region, could be a Zr_x(Fe, Cr, Ni, Be)$_y$ intermetallic. This intermetallic is similar to the one in spot 2 of Fig. 13, but the Zr content is lower; this difference is possibly caused by Zr being consumed in the reaction with BeO to form the reaction band (spot 3).

It was also observed in the solidified metal droplet that several non-soluble particles floated and segregated to the top (Fig. 14). The composition of these particles was Zr (58.0–63.0 at.%), O (33.0–35.0 at.%), and Fe (3.0–6.0 at.%). The presence of Be in these oxide particles cannot be ruled out. These compositions are similar to the chemistries that were observed in the ceramic reaction band (Fig. 13, spot 3). We can presume then that these particles are either precipitation products from the reduction of the beryllia by Zr or fragments that separated from the reaction band. Note that these particles did not interact with the metal alloy, nor were they wetted by it. This is consistent with the lack of wetting of the bulk metal on the reaction band (Fig. 10). This behavior was the same as that of the liquid metal that infiltrated the ceramic reaction band. There was also lack of bonding between the particles and the metal, similar to the separation of the metal droplet and the reaction band at the interface.

5. Conclusions

Chemical reactions were clearly observed at elevated temperatures in the Zr/BeO and HT9-15Zr/BeO systems. In both systems the Zr reduced the beryllia, and the beryllium and oxygen dissolved in zirconium. The molten metal did not completely wet the ceramic substrate. For the later system (HT-9-15Zr/BeO), in spite of the fact that a reaction or transition layer formed at the metal/ceramic interface, still there was no wetting. Thus, in this case, the concept of wetting as a parameter to assess indirectly the stability of a ceramic substrate in contact with a liquid metal at elevated temperatures is misleading.

As far as the primary mission of the tests, the use of BeO as a crucible material for Zr containing metal alloys is definitely not recommended above 1350°C. In our investigation we determined that BeO is not stable when exposed to Zr metal at elevated temperatures (>1600°C). The HT9-15Zr/BeO interface was different from the Zr/Be interface in its microstructural details, but the chemical reaction was similar. In both systems, Zr was active for reducing BeO. The chemical reaction was more extensive with pure Zr than with the HT9-15 wt% Zr alloy; for example, the depth of the liquid metal infiltration in the Zr/BeO system was eight times greater than in the HT9-15Zr/BeO system. This occurred even though the metal alloy become liquid much earlier than pure Zr, and so had more time to infiltrate the beryllia.

In summary the following are true:

1. In this investigation wetting proved to be a misleading indicator of the stability of a ceramic phase in contact with a liquid metal at elevated temperatures.
2. When selecting stable materials for service at high temperatures, thermodynamic data should be used with caution. According to the Gibbs free energy of formation, Zr should not reduce BeO, but our results showed significant dissolution of beryllia at temperatures near 1600°C.
3. For the Zr/BeO system there was no apparent change in the liquid/ceramic area of contact from the moment the drop was formed, but the original BeO interface was consumed. The molten Zr infiltrating the BeO could have caused the observed decrease in the contact angle and collapse of the metal droplet.

Acknowledgements

The authors would like to acknowledge Dr. A. Raraz and Dr. L. Leibowitz for helpful technical discussions and input into the manuscript, and the Analytical Chemistry Laboratory of the CMT Division at Argonne National laboratory for use of the SEM. The

U.S. Department of Energy under contract W-31-109-Eng-38 supported this work.

References

1. R. E. LOEHMAN, *American Ceramic Society Bulletin* **68** (1989) 891.
2. R. L. MEHAN and D. W. McKEE, *J. Mater. Sci.* **11** (1976) 1009.
3. R. L. MEHAN and R. B. BOLON, *ibid.* **14** (1979) 2471.
4. R. L. MEHAN and M. R. JACKSON, in "Materials Science Research," Vol. 14 (Plenum Press, New York, 1981) p. 513.
5. M. R. JACKSON, R. L. MEHAN, A. M. DAVIS and E. L. HALL, *Met. Trans.* **14A** (1981) 355.
6. D. UPHADYAYA, M. WOOD, C. M. WARD-CLOSE, P. TSAKIROPOULOS and F. H. FROES, *J. Metals* **46** (1994) 62.
7. S. M. FENG, J. M. YANG and J. A. GRAVES, *J. Materials Research* **8** (1993) 905.
8. J. H. GULPEN, A. A. KODENTSOV and F. J. J. VAN LOO, in "Applications of Thermodynamics in the Synthesis and Processing of Materials," edited by P. Nash and B. Sundman (1995). p. 127.
9. J. H. PEREPEZCO, M. H. DA SILVA BASSANI, J. S. PARK, A. S. EDELSTEIN and R. K. EVERETT, *Materials Science and Engineering* A **195** (1995) 1.
10. J. S. PARK, K. LANDRY and J. H. PEREPEZKO, *ibid.* **259** (1999) 279.
11. J. V. NAIDICH and G. M. NEVODNIK, *Inorganic Materials* **5** (1969) 1759.
12. K. NOGI and K. OGINO, *Trans. Japan Institute of Metals* **29** (1998) 742.
13. P. NIKOLOPOULOS, S. AGATHAPOULOS, G. N. ANGELOPOULOS, A. NAOUMIDIS and H. GRÜBMEIER, *J. Mater. Sci.* **27** (1992) 139.
14. C. RADO, S. KALOGEROPOULO and N. EUSTATHOPOULOS, in Materials Research Symposium Proc., Vol. 327 (1994) p. 319.
15. S. KALAGELOPOULO, L. BAUD and N. EUSTATHOPLOULOS, *Acta Metallurgica Materialia* **43** (1995) 907.
16. S. M. McDEAVITT, D. P. ABRAHAM and Y. P. PARK, *J. Nuclear Materials* **257** (1998) 21.
17. G. ECONOMOS and W. D. KINGERY, *J. Amer. Ceram. Soc.* **36** (1953) 403.
18. P. R. CHIDAMBARAM, A. MEIER and G. R. EDWARDS, *Materials Science and Engineering* A **206** (1996) 249.
19. D. CHATAIN, L. RIVOLLET and N. EUSTATHOPOULOS, *J. de Chim. Phys.* **83** (1986) 561.
20. J. J. BRENNAN and J. A. PASK, *J. Amer. Ceram. Soc.* **51** (1968) 569.
21. V. LAURENT, D. CHATAIN, C. CHATILLON and N. EUSTATHOPOULOS, *Acta Metall.* **36** (1998) 1797.
22. J. V. NAIDICH, V. M. PAREVERTAJLO and G. M. NEVODNIK, *Poroshk. Metallurg.* **45** (1972) 1025.
23. J. V. NAIDICH, in "Progress in Surface and Membrane Science," edited by D. A. Cadenhead and J. F. Danielli, Vol. 14 (Academic Press, New York, 1981) p. 353.
24. L. RAMQVIST, *Intern. J. Powder Metall.* **1** (1965) 2.
25. J. V. NAIDICH, *Russian Journal of Physical Chemistry* **42** (1968) 1023.
26. J. A. PASK, *Ceram. Bull.* **66** (1987) 1587.
27. M. G. NICHOLAS, *British Ceramic Transactions Journal* **85** (1986) 144.
28. N. EUSTATHOPOULOS and A. MORTENSEN, in "Fundamental of Metal-Matrix Composites," edited by S. Suresh, A. Mortensen and A. Needleman (Butterworth-Heinemann, London, 1993) p. 42.
29. D. CHATAIN, L. COUDURIER, A. STEICHEN and N. EAUSTATHOPOULOS, in "Interfaces in New Materials," edited by P. Grange and B. Belmon (Elsevier Applied Science, London, 1991) p. 210.
30. V. MERLIN, P. KRITSALIS, L. COUDURIER and N. EUSTATHOPOULOS, in Proc. MRS Fall Meeting, Boston, MA (Materials Research Society, Pittsburgh, PA, 1992) Vol. 238, p. 475.
31. C. B. ALCOCK, K. T. JACOB and S. ZADOR, *Atomic Review*, special issue no. 6, edited by O. Kubascnewski (1976) p. 7.
32. R. A. ROBIE, B. S. HEMINGWAY and J. R. FISHER, in *Geological Survey Bulletin* 1452 (United States Department of the Interior, 1978).
33. Binary Alloy Phase Diagrams, 2nd ed., Vol. 3 (ASM International, 1990) p. 2941.
34. Binary Alloy Phase Diagrams, 2nd ed., Vol. 1 (ASM International, 1990) p. 717.
35. B. J. KEENE, *Intl. Materials Review* **38** (1993) 157.

Received 11 January 2001
and accepted 29 March 2002